Parametrisation of a rolling resistance model for extending the brush tyre model

Lisa Ydrefors*

VTI, Swedish National Road and
Transport Research Institute,
Linköping, S-58195, Sweden

and

Division of Vehicle Dynamics,
Department of Engineering Mechanics,
KTH Royal Institute of Technology,
Stockholm, S-10044, Sweden
Email: lisa.ydrefors@vti.se
*Corresponding author

Martin Åsenius and Hugo Jansson

Department of Electrical Engineering,
Linköping University,
Linköping, S-58183, Sweden
Email: martin.asenius@hiq.se
Email: jansson1994@gmail.com

Sogol Kharrazi and Mattias Hjort

VTI, Swedish National Road and
Transport Research Institute,
Linköping, S-58195, Sweden
Email: sogol.kharrazi@vti.se
Email: mattias.hjort@vti.se

Jan Åslund

Department of Electrical Engineering,
Linköping University,
Linköping, S-58183, Sweden
Email: jan.aslund@liu.se

Abstract: A rolling resistance model (RRM) has been created and parametrised with the purpose of modelling tyre rolling resistance within complete vehicle dynamics simulations. The RRM is based on a combination of the Masing and Zener models to simulate the Payne effect and the viscoelastic properties of rubber. The parametrised model is able to recreate the relationship between the rolling resistance and the tyre deformation well and it has a low computational

power requirement. Today the model is limited to simulation of free-rolling tyres on a flat surface, but it can be extended to also include the effects of changes in operating conditions such as wheel angles or road surface.

Keywords: rolling resistance; parametrisation; vehicle dynamics simulation; wheel load; tyre deformation; tyre modelling; tyre temperature; Zener model; Masing model.

Biographical notes: Lisa Ydrefors is a PhD-student at VTI, The Swedish National Road and Transport Institute, and KTH Royal Institute of Technology in Sweden. She is also connected to the Centre for ECO2 Vehicle Design. She received her Master's degree in Engineering Physics from Chalmers University of Technology in Sweden in 2006, with focus on Matter and Materials. Her research focus is on rolling resistance, both in terms of measurement methods and modelling.

Martin Åsenius carried out his Master's thesis on Parametrisation of the Model presented in this paper at VTI. In the thesis work, the influence of temperature in real driving scenarios was also investigated. He graduated from Linköping University in Sweden in 2021 with a Master's degree in Electrical Engineering with focus on modelling and control theory.

Hugo Jansson carried out his Master's thesis on Parametrisation of the Model presented in this paper at VTI. In the thesis work, the influence of temperature in real driving scenarios was also investigated. He graduated from Linköping University in Sweden in 2021 with a Master's degree in Electrical Engineering with focus on modelling and control theory.

Sogol Kharrazi received her Bachelor's degree in Mechanical Engineering from Sharif University of Technology in Iran. She got a Master's degree in Automotive Engineering in 2005, and a PhD in Machine and Vehicle Systems in 2012, both from Chalmers University of Technology in Sweden. She is currently a Senior Researcher at VTI, the Swedish National Road and Transport Research Institute. She also works as an Adjunct Associate Professor at Department of Electrical Engineering at Linköping University. Her research interests include tyre and vehicle dynamics.

Mattias Hjort received a Master's degree in Applied Physics and Electrical Engineering from Linköping University in Sweden in 1997, and a PhD in Computational Physics from the same university 2001. He is currently a research leader at VTI, the Swedish National Road and Transport Research Institute, and has a particular interest in the field of tyre road interaction.

Jan Åslund received a Master's degree in Mechanical Engineering and a PhD in Applied Mathematics from Linköping University in Sweden in 1996 and 2002, respectively. He is currently an Associate Professor at the Department of Electrical Engineering at Linköping University. His research interests include vehicle dynamics, optimal control, model-based diagnosis, and motion planning.

1   Introduction

The latest Intergovernmental Panel on Climate Change report (Masson-delmotte et al., 2021) describes large ongoing global climate changes. To counteract a continuation of such changes, the emissions of greenhouse gases, such as CO_2, must be reduced. A large contributor of CO_2-emissions is the transport sector. During 2018, and only within EU, this sector emitted 1.1 million tonnes of CO_2 equivalents. 72 % of those emissions are originating from road transports (EU, 2019).

One of the contributing factors to road transport's emissions is the rolling resistance of tyres. Rolling resistance is an energy loss within the tyres that has been defined as "mechanical energy converted into heat by a tyre moving for a unit distance on the roadway" (Schuring, 1977). In many applications, for example, free-rolling tyres on a flat surface, this energy loss per distance can be treated as a force that acts against the direction of travel. This view is common for both rolling resistance tests and simulations. The rolling resistance of a tyre is determined by several different factors, such as its geometry, material properties, driving conditions and the road surface (Aldhufairi and Olatunbosun, 2018; Ydrefors et al., 2021a).

To increase the understanding of rolling resistance and how it is affected by these different determining factors and their interactions, rolling resistance simulations is an important tool. Many good simulation models exist today, for example complex models such as finite elements method (FEM) models (Ghoreishy, 2008). These models give accurate results, provided that the model parameters are set correctly. However, the large number of parameters needed to be set in these models, makes the parametrisation process complicated. Achieving a good parametrisation requires detailed information about the constituent parts of the tyre, which is often classified by the manufacturers. Another drawback of these models is their high demand for computational power, which prevent an efficient usage of them as part of a complete vehicle dynamics simulation. These simulations can be used to study the interactions between the tyre rolling resistance and different vehicle manoeuvres, for instance, effects of vehicle settings, such as wheel load, camber or toe angles on tyre rolling resistance.

The overall aim with this work is to create and parametrise a mathematical model for rolling resistance simulations that can be used as a submodel in complete vehicle models. The rolling resistance model (RRM) should be based on physical relationships, to enable calculations of how the rolling resistance variations connects to changes in vehicle settings such as wheel load or wheel angles. A model that estimates the rolling resistance moment from individual points in the contact area would also result in a better prediction of the dynamic load distribution. The latter would be of great value for subsequent modelling of the friction forces between tyre and road. Finally, the RRM shall be parameterised using measurement results from a rolling resistance test equipment.

A commonly used model for tyre friction forces is the so-called brush tyre model. The tyre contact surface is divided into small brush elements, extending laterally over the full contact region width, but with infinitesimal length in the longitudinal direction. Using just a few model parameters for the rubber properties combined with a simple load distribution allows for analytical expressions of the friction forces (Svendenius, 2007). More advanced rubber models or load distributions may require numerical methods

for solving the equations, in which case a finite number of brush elements, or bristles, is used.

In this work, a RRM has been created, where the tyre carcass is subdivided in a way that allows for the model to be used in combination with the brush tyre model, providing a useful extension of the same (Jansson and Åsenius, 2021). The model is inspired by previous work by Conte and Davari (Conte, 2014; Davari, 2015), and has been parametrised using rolling resistance measurements from a flat track equipment. This model uses the load dependent tyre deformation to calculate the rolling resistance. The developed model presented in this paper is limited to calculations of rolling resistance for a free-rolling tyre on a flat road rolling straight forward but can be extended to also include wheel angles or unevenness of the road. The outline of the paper is as follows. First, the developed tyre model is explained. This is followed by a description of the test facility and of the performed tests and then the parameterisation. Finally, the discussion, conclusions and some recommendations for future work are presented.

2   Tyre model

The common brush tyre model is built up by a single line of bristles modelled as linear springs on a stiff carcass, which bend longitudinally and laterally. The vertical force on each bristle is determined by a specified load distribution, often parabolic and symmetric with respect to the centre of the tyre. In the model created in this work the tyre carcass is flexible in the radial direction, and in order to be compatible with the brush tyre model the tyre is subdivided into radial slices attached at the rim. The carcass is assumed to be stiff in the lateral direction, and since there is no lateral slip or camber there is no need for a lateral subdivision. Each slice can be compressed in the radial direction which creates the vertical force acting on the corresponding bristle in the brush tyre model. Although technically these slices are not bristles in the same sense as in the brush tyre model, we will use the same nomenclature for the slices due to the close connection to the brush tyre model.

The bristles rotate with the tyre. The angular position relative to the centre of the contact patch, φ for a bristle is updated in each time step and depends on the velocity of the tyre. Figure 1 illustrates the bristle deformation. The symbol δ represents the vertical deformation of the tyre and δ_i, the vertical deformation of the ith bristle. With the proposed RRM it is possible to model how the tyre is affected by the road unevenness. The forces and deflections are modelled using springs, dampers and corresponding geometry. The model uses the tyre deformation, δ, as input to calculate the vertical forces. To determine the deformation for a specific wheel load an iterative process is needed. The forces acting on the tyre together with the different radii are illustrated in Figure 2. R_u is the unloaded tyre radius and R_l the loaded tyre radius. The effective rolling radius R_e is the ratio of the linear velocity of the wheel centre in the x-direction and the angular velocity of the wheel (SAE International, 1976). This results in an effective rolling radius between R_u and R_l. If the angular velocity is unknown, the effective rolling radius has to be estimated, or if possible, measured.

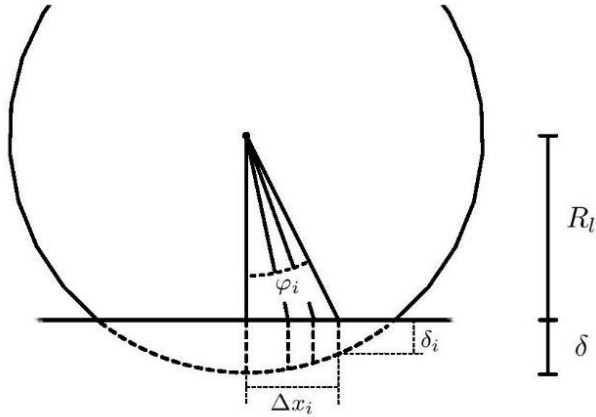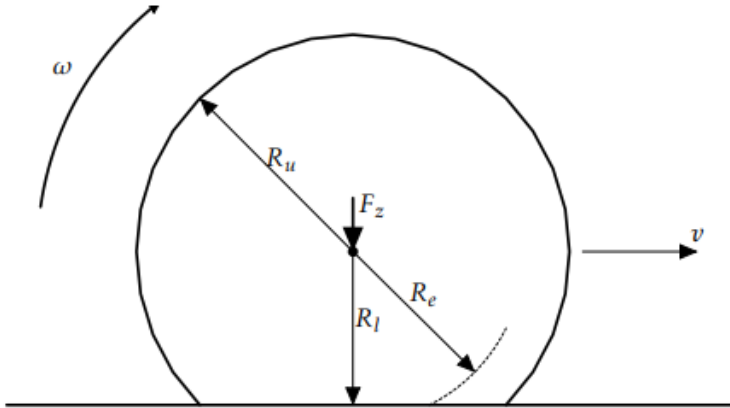**Figure 1**   Illustration of the bristle deformation size


Figure 2   Definition of tyre radius

The bristle model aims to capture the behaviour of the tyre where a deflection includes many separate effects such as shearing and compression of the tread, bending of the sidewall and reduction of the interior volume. It is postulated that each bristle can be treated as a viscoelastic element and that the model must take into account both the frequency dependent and frequency independent behaviour of rubber. This is achieved using two models in parallel, the Zener viscoelastic model (Zener, 1948) and the Masing friction model (Masing, 1923), as has previously been done by Conte (2014).

The Zener model consists of a spring in parallel with a spring and a damper in series, a so-called Maxwell element, and contains the model parameters k_1, k_2 and c. The aim of the Zener model is to describe the viscoelastic properties of the tyre. The Masing model is built up by a number of parallel Jenkins elements. A Jenkins element consists of a spring in series with a Coulomb friction element, and the model contains the parameters k_3 and ϱ, as shown in Figure 3. More Jenkins elements in the Masing model provides a better representation but increase the number of model parameters with two per element, which complicates the parameter identification process. For simplicity one single Jenkins element was chosen to represent the internal friction in this work. The aim of the Masing

model is to capture the Payne effect, also known as the Fletcher-Gent effect, which describes how the stiffness of a filled rubber decreases as the deformation amplitude increases (Payne, 1962).

Figure 3 The bristle model built up by the Zener model with the parameters k_1, k_2 and c, marked by a red frame, and the Masing model with the parameters ϱ and k_3 (see online version for colours)
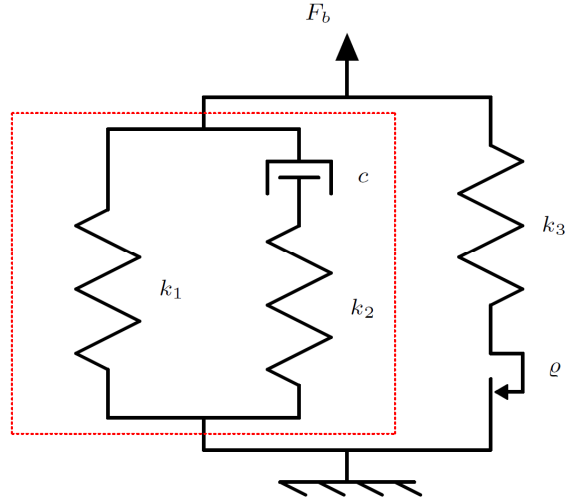
The resulting vertical force acting on each bristle, F_b, is the sum of the contribution from both the Zener and Masing models, according to

$$F_b = F_{ve} + F_f \tag{1}$$

where F_{ve} is the Zener viscoelastic force and F_f is the Masing friction force. The summation of the force in all the bristles gives the total force acting on the tyre. Likewise, the resulting rolling resistance is given by the sum of all bristle's contributions to a rolling resistance moment, divided by the loaded tyre radius. See equations (2) and (3), which present the calculation of the vertical force, F_Z, and rolling resistance, RR, where Δx_i is the horizontal distance from bristle i to the centre of the tyre.

$$F_Z = \sum_i F_{b,i} \tag{2}$$

$$RR = \sum_i F_{b,i} \Delta x_i / R_l \tag{3}$$

The force from the Masing model, F_f, is governed by

$$\dot{F}_f = \begin{cases} k_3 \dot{\delta}_i, & |F_f| < \varrho \\ k_3 \dot{\delta}_i, & |F_f| = \varrho \text{ and } \mathrm{sgn}\left(\dot{\delta}_i \cdot F_f\right) \le 0 \\ 0 & \text{else} \end{cases} \tag{4}$$

The absolute values, logical expression, and sign function in Equation 4 ensure that the internal friction force remains within its boundaries: $-\varrho \leq F_f \leq \varrho$. The corresponding static F_f, for a non-moving loaded tyre is min $(k_3\delta_i, \varrho)$. The force contribution from the Zener viscoelastic model in the time domain is

$$F_{ve}^{t+\tau} = \frac{\left((2c - k_2\tau)\cdot F_{ve}^t + \left(k_1k_2\tau + c\left(k_1 + k_2\right)\right)\delta_i^{t+\tau}\cdot + \left(\tau k_1k_2\right)\delta_i^t - c\left(k_1 + k_2\right)\cdot\delta^{t-\tau}\right)}{\left(2c + k_2\tau\right)} \quad (5)$$

where τ is the time step. The force is calculated using the deformations during three different timesteps and the achieved viscoelastic force from the previous time-step. The corresponding static force F_{ve}, for a non-moving loaded tyre is $F_{ve} = k_1\delta_i$. Besides the mentioned parameters k_1, k_2, c, k_3 and ϱ, the model also requires either the wheel load, F_Z, or the loaded tyre radius, R_l as input. During the parameter optimisation process, described in Chapter 4, R_l is used as an input parameter and F_Z is calculated. For the effective rolling radius, the estimate

$$R_e = \sqrt{\frac{R_u^2 + 3R_l^2}{4}} \quad (6)$$

from Moore (1975) for free-rolling tyres, has been used. The deformation of each bristle is derived through geometry by using their angular position, the loaded and the unloaded tyre radius. This deformation is used to calculate the force on each bristle. The resulting bristle model is presented in Figure 3, where the red frame marks the Zener model.

As mentioned earlier, tyre deformation is the model input. How the different parameters affect the modelled wheel load and rolling resistance for a given tyre deformation is summed up in Table 1. The speed independent part of the rolling resistance is governed by the two Masing parameters, while the viscoelastic parameters k_2 and c dictates the speed dependent part. The elastic part of the Zener model, parameter k_1, determines the static load distribution, together with the Masing parameters. Due to the symmetry of the tyre deformation, k_1 will not contribute to the rolling resistance for a given tyre deformation (it has a minor effect as is described in the discussion section). For a specific wheel load, however, k_1 will have a large impact on the rolling resistance since it determines the deformation.

**Table 1**   Parameter influence for a given deformation

Load: static tyre	k_1, k_3, ϱ
Load: rolling tyre	k_1, k_2, c, k_3, ϱ
RR: speed independent part	k_3, ϱ
RR: speed dependent part	k_2, c

3   VTI tyre test facility

The VTI tyre test facility is used to obtain the measurement data needed to parametrise the model. This test facility is a flat beam test equipment, used for measurements of tyre forces under controlled conditions, see Nordström (1993) for a detailed description. The

tyre is fixed in a rig and pressed against a metal beam, which represents the road, at a set wheel load, see Figure 4. Besides using the steel surface of the beam as road surface, other surfaces such as asphalt and ice can also be used. The beam is moved beneath the fixed tyre with a maximum speed of 36 km/h. Piezoelectric sensors are used to measure the forces acting on the tyre in the lateral, longitudinal and vertical directions.

Figure 4   VTI tyre test facility (see online version for colours)
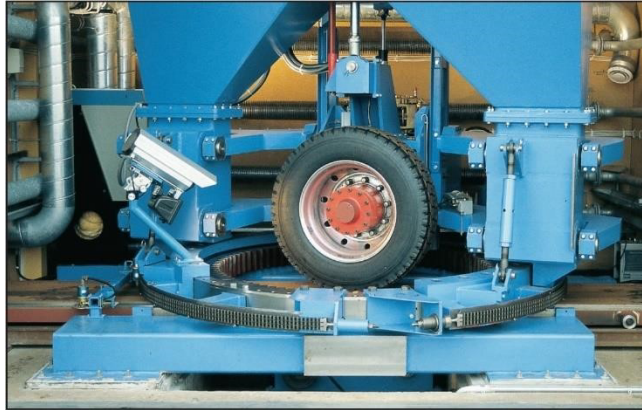
Source: Nordström (1993)

The VTI tyre test facility can be used for rolling resistance measurements (Ydrefors et al., 2021b). Since the tyre temperature affects the rolling resistance, the tyre temperature must be controlled. The tyre temperature is measured on the tyre surface. In the tread area, the temperature is measured on both the outside and inside surface of the tyre. The sidewall temperature is measured on the inside surface. If needed, the tyre is heated to the requested measurement temperature by running the tyre on a rotating cylinder. It is then let to cool down until the gradient between the inside and outside tyre tread surface temperature vanishes. When this measurement temperature is reached, the steel beam is launched, and a measurement of the tyre forces is made.

The longitudinal tyre force gives the rolling resistance, but it also includes the normal force alignment error and the parasitic loss (energy losses within the equipment such as bearing losses). They both originate from the measurement equipment and are subtracted from the measurement to obtain the rolling resistance.

A sensor is continuously logging the vertical position of the tyre, leading to accurate measurements of the tyre deformation for both a static and rolling tyre. The effective rolling radius is obtained for low speed conditions by measuring the travelled distance when the tyre rolls a certain number of revolutions.

The measurements were conducted on two all-season passenger car tyres of dimension 235/50R19, one class A and one class B tyre, both with a capped inflation pressure of 2.8 bar, set at 18°C ambient air temperature. A class A tyre shall according to its labelling have lower rolling resistance than a class B tyre.

The rolling resistance was measured at three speeds, 1.7 km/h, 10 km/h and 30 km/h, and at five wheel loads: 300 kg, 400 kg, 500 kg, 600 kg and 700 kg. The tests on the class B tyre were performed at two different tyre temperatures while for the class A tyre the tests were only performed at the lower temperature.

The intention was to maintain constant tyre temperatures, but the temperature varied between 33.6°C and 37.8°C for the warmer tyre measurements and between 14.9°C and 18.7°C for the colder tyre measurements. These variations are due to room temperature variations and limitations in available test time. The deviation in tyre temperature from the intended temperatures causes difficulties in the parametrisation of the RRM. It is unclear to which extent the parameter values are affected by these temperature deviations. Due to the limitations in test time, the same measurement results were used for both the parameterisation of the model as well as the comparative experimental results.

4 Parameterisation

The gained test data was used to optimise the model parameters k_1, k_2, c, ϱ and k_3, in such a way that the model would comply with the data. This was achieved with a cost function, according to

$$g = \sum_{m=1}^{n}\left(\frac{F_{Z,m} - \hat{F}_{z,m}}{F_{Z,mean}}\right)^2 + \sum_{m=1}^{n}\left(\frac{RR_m - \widehat{RR}_m}{RR_{mean}}\right)^2 \tag{7}$$

where n is number of measurements, $F_{Z,m}$ and RR_m are the measured wheel load and rolling resistance, with $\hat{F}_{z,m}$ and $\widehat{RR}_m$ being the corresponding values estimated by the model. The optimised model parameters are those which minimise the cost function.

To avoid identifying local minimums instead of global, a global optimisation procedure was used. It was implemented by repeated use of the local optimisation algorithm with random start parameters, to find a global minimum. The values of the resulting optimised parameters are found in Table 2.

Table 2   Parameters obtained for different tyres and temperatures for 1 rad of the tyre circumference

Tyre	Zener			Masing	
	k_1 $\left(\dfrac{kN}{m\,rad}\right)$	k_2 $\left(\dfrac{kN}{m\,rad}\right)$	c $\left(\dfrac{Ns}{m\,rad}\right)$	ϱ $\left(\dfrac{N}{rad}\right)$	k_3 $\left(\dfrac{kN}{m\,rad}\right)$
Cold Class A	472.9	92.65	91.48	252.0	123.7
Cold Class B	487.6	97.59	114.7	350.8	114.7
Warm Class B	518.4	125.4	71.91	348.6	103.1

As seen in Table 2, the parameter k_1 is smaller for cold tyres, which indicates that the stiffness is lower for cold tyres. This correlates with the measurement data, since the deflection is larger for the cold tyre compared to the warm tyre, as can be seen in Figure 5. At first sight this may seem contradictory, since at a constant air pressure a

warm tyre has a lower stiffness than a cold tyre. However, the measurements were made with capped inflation pressure, which means that the amount of air in the tyre is kept constant, leading to increased inflation pressure as the temperature is rising and thus also increased tyre stiffness. The deflection for the warm class B tyre is 3.8% smaller than for the cold class B tyre, while the inflation pressure is 4.9% larger for the warm tyre. The larger difference in inflation pressure effectively compensates for the softer rubber of the warmer tyre.

Figure 5   Tyre deformation for class B tyre (static measurement) (see online version for colours)
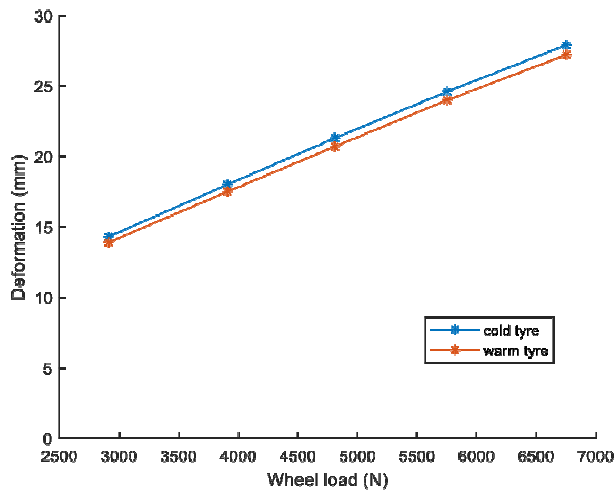
The number of bristles used, influences the value of the optimised parameters. By increasing the number of bristles, the tyre volume each bristle represents decreases, resulting in higher accuracy, but also higher demand on computational power. Table 3 gives the mean absolute percentage error (MAPE) for the deviation of the model, with 150 bristles, from the measured values of wheel load and rolling resistance.

Table 3   MAPE for the simulations from the different test series

Tyre	F_Z (%) MAPE	RR (%) MAPE
Cold Class A	5.66	4.17
Cold Class B	5.04	3.89
Warm Class B	4.66	2.04

The results indicate that the modelled load and rolling resistance are more accurate for the class B tyre than for the class A tyre and more accurate for a warm tyre than a cold tyre. In Figures 6 and 7 the measured load and rolling resistance are plotted together with their modelled counterpart, vs. the tyre deformation. While the model captures the general behaviour of the rolling resistance at different tyre deformations well, it is clear that the relationship between the wheel load and the deformation is not accurately described.

Figure 6   The measured and modelled wheel load against deformation for the cold class B tyre
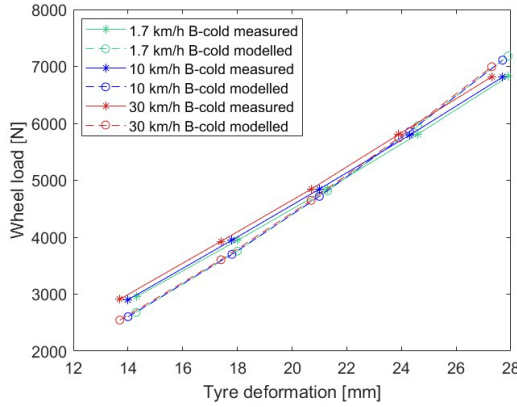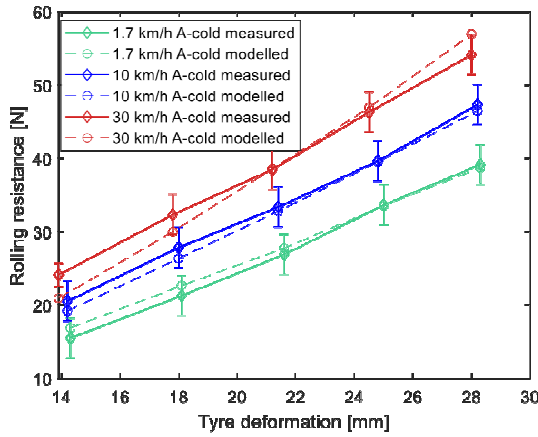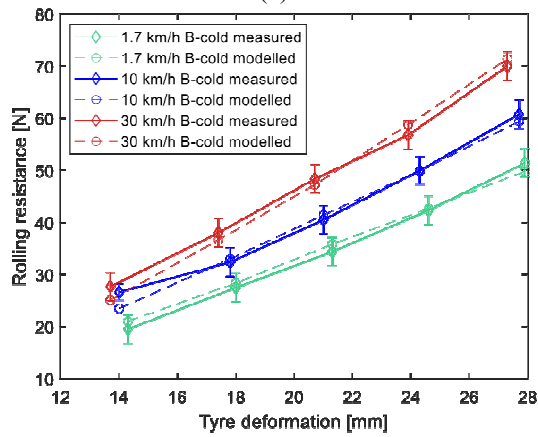(see online version for colours)

Figure 7   The measured and modelled rolling resistance against deformation for the three studied
cases. The error bars indicate the measurement uncertainties: (a) cold class A tyre;
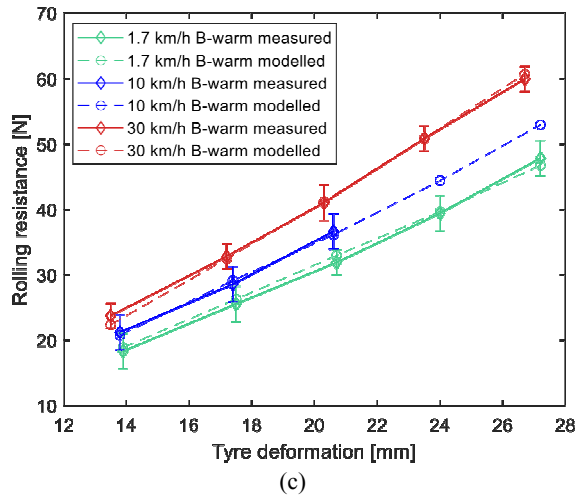(b) cold class B tyre and (c) warm class B tyre (see online version for colours)

(a)

(b)

Figure 7 The measured and modelled rolling resistance against deformation for the three studied cases. The error bars indicate the measurement uncertainties: (a) cold class A tyre; (b) cold class B tyre and (c) warm class B tyre (see online version for colours) (continued)

(c)

Also, the measurement results in Figure 6 indicate that an increase in test speed corresponds to a small decrease in tyre deformation, but this is not visible in the modelled data.

In the following discussion the RRM is evaluated only with respect to deformation instead of wheel load. Due to the apparent inaccuracies of the wheel load estimation, evaluating the modelled rolling resistance as a function of wheel load would not be useful at this point.

5   Discussion

The proposed model uses the tyre deformation to calculate the corresponding wheel load and rolling resistance. It manages to model the rolling resistance-deformation relationship well, while the fit for the wheel load-deformation relationship between measured and modelled values is not that good. An explanation could be that the model simulates the tyre deformation as a pure compression of the tyre bristles together with the contained air, where the corresponding force is linear with respect to the deformation. The measured deformation is however quite large and will also include bending of both sidewalls and tread. It is plausible that the elastic properties of the bending may not be accurately described by a linear compression model.

In the current model, the wheel load force arising from the elastic spring k_1 will be proportional to the total deformed area (indicated by the dotted line in Figure 1). The deformed area as a function of deformation is plotted in Figure 8 together with static measurements of the wheel load. The area has been scaled by k_1 and thus represents the vertical force. While the measured data indicate a rather linear relationship between wheel load and deformation, the deformed area is obviously nonlinear. Hence, it is clear that regardless of the choice of k_1, the model cannot capture the linear relationship

between the wheel load and the tyre deformation and the model needs to be improved in this regard. This deviation is also seen in Figure 6, where the difference in inclination of the modelled and measured wheel load-deformation relationship shows the same trend as in Figure 8. This is to be expected since the elastic part of the model almost entirely determines the wheel load for the investigated speed range. In theory, the wheel load-tyre deformation relationship also depends on the Masing parameters, ϱ and k_3, but their contribution is deemed as negligible, compared with k_1, as illustrated in Figure 9.

Figure 8   Relationship between wheel load and tyre deformation for the cold class B tyre (see online version for colours)
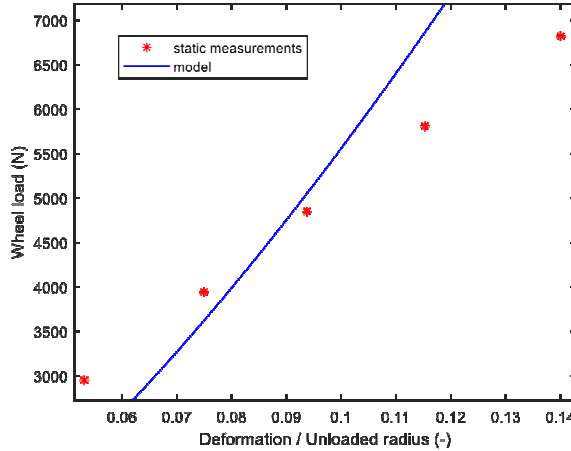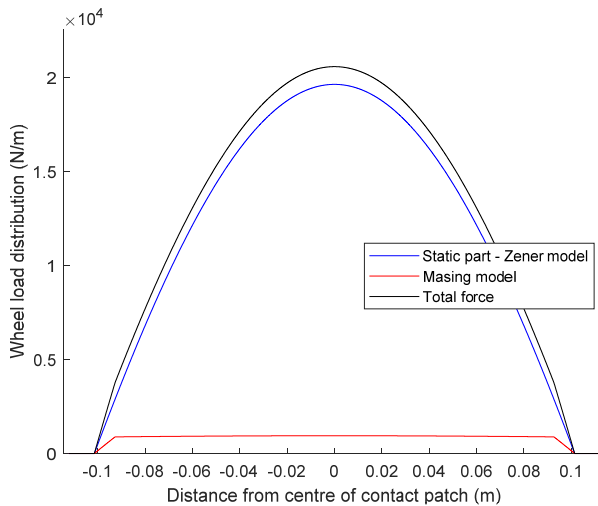

Figure 9   Contribution to static load for the cold class B tyre from the different parts of the model (see online version for colours)

Beside the wheel load distribution, the parameters ϱ and k_3 also influence the rolling resistance of the tyre, independently of the tyre speed. The parameter ϱ determines the maximum force that can be extracted from the Jenkins element while k_3 governs the

relationship between the deformation and the force within the element. If the maximum force never is reached, this element will not actively contribute to the rolling resistance, but it will affect it in the same way as k_1 since it will function as a pure spring with an even force distribution around the wheel centre. A small k_3/ϱ, shown in Figure 10, gives a close to symmetrical force distribution from the Jenkins element around the centre of the tyre contact patch. Therefore, the contribution to the rolling resistance will be small. A larger k_3/ϱ ratio, will increase the rolling resistance.

Figure 10 Wheel load from Masing model, for a rolling tyre (see online version for colours)
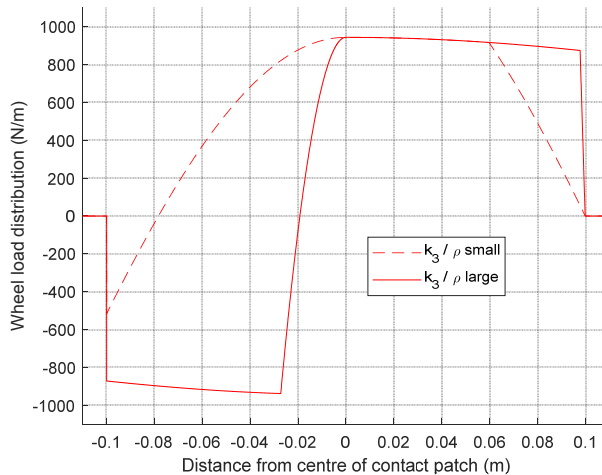
The remaining parameters, k_2 and c, from the Maxwell element in the Zener model, state the viscoelastic properties of the tyre. Figure 11 shows how the rolling resistance varies for different values on the parameters. This effect is speed dependent, but generally the maximum rolling resistance is found using the largest values for both parameters. The rolling resistance plot shows a ridge, where its placement is speed dependent. At the lowest speed (Figure 11(a)), the ridge is found at small c- and large k_2-values. As the speed increases, this ridge shifts toward larger c- and smaller k_2-values. The ridge placement at low test speeds results in a small influence of the c parameter, except at highest k_2-values. Consequently, the Zener rolling resistance is mainly governed by k_2 at low speeds. At higher speeds, the rolling resistance will exhibit a peak as a function of k_2, and further increase of this parameter will lead to a diminishing rolling resistance. The position of the peak is determined by the c-parameter, where a lower c leads to a peak at a lower k_2-value.

The total rolling resistance is the sum of the Zener and Masing rolling resistance, where both parts originate from asymmetry in the wheel load distribution. In the end of the contact patch, both the Masing model and the dynamic part of the Zener model gives a negative contribution to the wheel load distribution. Since a negative wheel load is unrealistic, the wheel load distribution is set to zero, where the sum of the forces becomes negative, see Figure 12. The magnitude of k_1 affects where this zero crossing occurs and hence indirectly influences the rolling resistance. For a given tyre deformation, k_1 does not contribute to rolling resistance directly, since its resulting force is symmetrical around the centre of the tyre contact patch.

Figure 11 Rolling resistance modelled with the Zener model using different k_2 and c – values for the cold class B tyre. The red point shows the values used in the model: (a) simulated test speed 1.7 km/h and (b) simulated test speed 80 km/h (see online version for colours)

(a)

(b)
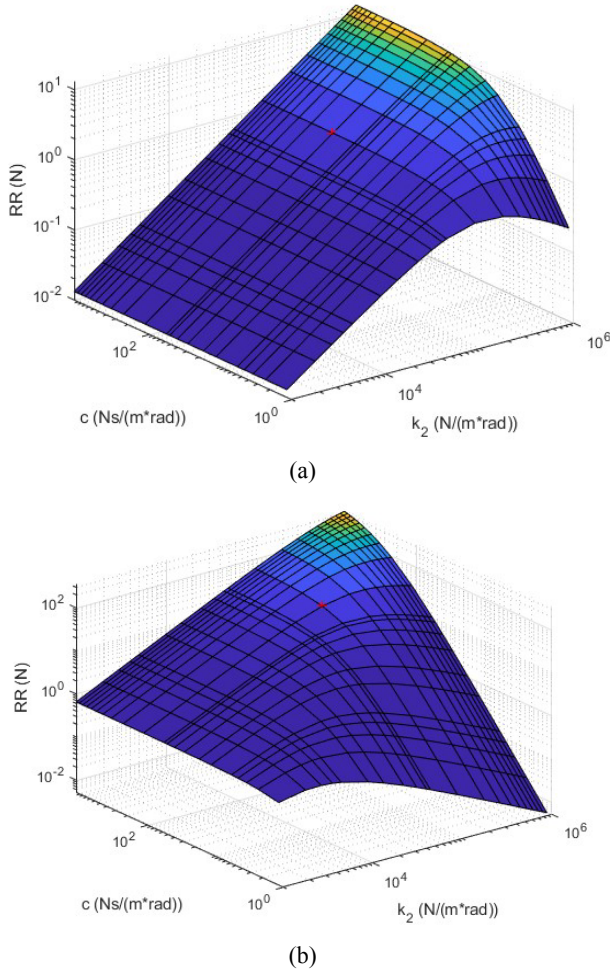
The Masing model contributes with a larger share of the rolling resistance than the Zener model for the tested tyres at the measured speeds, which is seen in Table 4. The Zener model should, however, dominate the rolling resistance at higher speeds since its influence increases with speed. This is exemplified through including results of a rolling resistance simulation with the estimated model parameters, at a speed of 80 km/h, in Table 4.

The used model connects the viscoelastic effect in the Zener model with the Payne effect modelled in the Masing model. The Payne effect is caused by fillers in the rubber and the estimated rolling resistance originating from this effect by the model is smaller for the class A tyre compared to the class B tyre. This indicates that the tyre industry's efforts to reduce rolling resistance through a reduction of fillers, as well as using new

filler materials have been successful. Considering that the Masing model contributes to a large portion of the rolling resistance, the effect of the number of Jenkins elements needs to be further investigated.

Table 4 The rolling resistance from the Masing and Zener models. The rolling resistance from the dynamic part of the Zener model is presented at four different speeds, both as absolute values and as its share in the total rolling resistance

	Masing model (N)	*Zener model* (N)				*Share of Zener model in the total rolling resistance* (%)			
Speed (km/h)	–	1.7	10	30	80	1.7	10	30	80
Cold class A tyre	16.6	0.7	3.7	10.2	21.3	4.0	18.2	38.1	56.2
Cold class B tyre	20.5	0.8	4.6	12.4	24.5	3.8	18.3	37.7	54.4
Warm class B tyre	19.6	0.5	3.0	8.5	19.7	2.5	13.2	30.2	50.1

Figure 12 Modelled F_Z distribution for the cold class B tyre, with the speed dependant part of the model at two different speeds. A closeup of the lower left part of the graph is shown in the inset (see online version for colours)
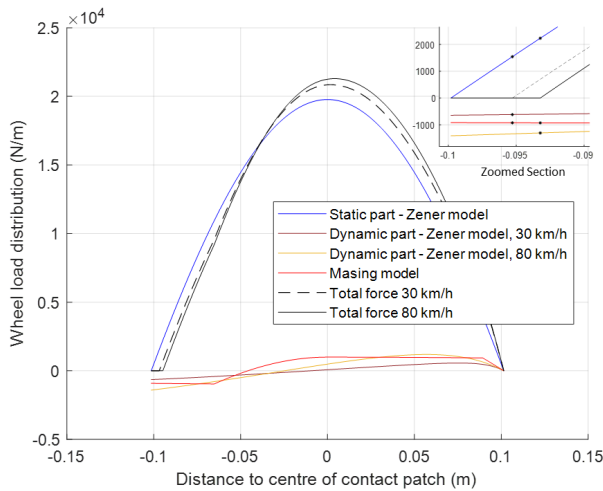
The rolling resistance from the Zener model is also affected by how the effective tyre radius, R_e, is estimated. Equation (6) shows that R_e is directly affected by the deformations. To determine the accuracy of this estimation, the effective rolling radius for the class A tyre was measured. The estimated effective rolling radius was found to only deviate about 2% from the measured rolling radius, which indicates that the used estimation is good.

Another factor which affects the modelled rolling resistance is the accuracy of the rolling resistance measurements used to parametrise the model. This accuracy, found in (Ydrefors, 2021b), is included as error bars on the measurement result in Figure 7. The size of the error margins is due to the tyre temperature variations and that each point is the average of only small number of measurements that have been considered. For the cold B-tyre, the tyre temperature remained within $16.3°C \leq Ttyre \leq 18.4°C$. The other tyres had larger temperature variations.

The rolling resistance simulated from the model is mostly found within the error margins for the measurements. The error margins are relatively large, an increased number of measurements performed at a more stable temperature would result in smaller error margins.

Although there are tendencies that the rolling resistance as a function of tyre deformation deviates between model and measurements at the highest speed, the discrepancies are within the error margins. Besides the measurements, the setup of the cost function also affects the resulting rolling resistance. The model parameters are identified through optimisation with a cost function, which includes the cost of rolling resistance and wheel load deviations between modelled and measured values. These costs have been weighted as equally important. If one is deemed as more important, it could be given a higher weight in the optimisation which would make it more influential and affect the resulting rolling resistance from the model.

Despite some shortcomings in the current version of the proposed RRM, it shows encouraging results to be further developed. Also, similar semi-physical models have been shown to be valuable for simulations of the effects of different wheel settings on the rolling resistance (Davari, 2015), which encourage continuation of development of the proposed model.

The fit between the modelled and measured rolling resistance – deformation relationship is good, and future efforts should focus on further adjustment of the relationship between the wheel load and the tyre deformation.

6   Conclusions and further work

This work describes the development and parametrisation of a RRM with the purpose to be used as a submodel within complete vehicle dynamics simulations. The parameterised RRM was found to fit the measured value well for the relationship between rolling resistance and tyre deformation. However, the fit is not as good for the relationship between wheel load and tyre deformation, which depends on the model geometry. An analysis of the modelled values showed that the largest difference between the cold class A and cold class B tyre is a reduction in the rolling resistance contribution from the Payne effect in the Masing model. If the cold class B tyre instead is compared to the warm class B tyre, the difference can be attributed to the viscoelastic rolling resistance part of the Zener model, which is lower for the warm tyre.

One suggestion for future work is to include slip and longitudinal deflection to gain a parametrised extended brush tyre model. Another suggestion for future work is to examine if the model could be modified so that the relationship between wheel load and tyre deformation resembles reality better. Effect of using just one Jenkins element in the Masing model should also be investigated.

Further suggestions for future work are to include the effect of different wheel angles on rolling resistance and to extend the parametrisation process to include this effect. To include the influence of driving torque or tyre temperature on the rolling resistance into the model, would also be another valuable improvement.

Acknowledgements

References

Aldhufairi, H.S. and Olatunbosun, O.A. (2018) 'Developments in tyre design for lower rolling resistance: a state of the art review', *Proceedings of the Institution of Mechanical Engineers, Part D: Journal of Automobile Engineering*, Vol. 232, No. 14, pp.1865–1882.

Conte, F. (2014) *Expanding the Brush Tire Model for Energy Studies*, Master thesis, KTH Royal Institute of Technology, Stockholm, Sweden.

Davari, M.M. (2015) 'Extended brush tyre model to study rolling loss in vehicle dynamics simulations', *International Journal of Vehicle Design*, Vol. 73, No. 4, pp.255–280.

EU (2019) [online] https://www.europarl.europa.eu/news/en/headline s/society/20190313STO31 218/co2-emissionsfrom-cars-facts-and-figures-infographics/

Ghoreishy, M.H.R. (2008) 'A state of the art review of the finite element modelling of rolling tyres' *Iranian Polymer Journal*, Vol. 17, No. 8, pp.571–597.

Jansson, H. and Åsenius, M. (2021) *The Relation between Rolling Resistance and Tyre Temperature in Real Driving Scenarios*, Master thesis, Linköping University, Linköping, Sweden.

Masing, G. (1923) 'Zur heyn' schen theorie der verfestigung der metalle durch verborgen elastische spannungen', *Wiss. Veröff. SiemensKonzern*, Vol. 3, pp.231–239.

Masson-delmotte, V., Zhai, P., Pirani, A., Connors, S.L., Péan, C., Berger, S., Caud, N., Chen, Y., Goldfarb, L., Gomis, M.I., Huang, M., Leitzell, K., Lonnoy, E., Matthews, J.B.R., Maycock, T.K., Waterfield, T., Yelekçi, O., Yu, R. and Zhou, B. (2021) *IPCC, 2021: Climate Change 2021: The Physical Science Basis. Contribution of Working Group I to the Sixth Assessment Report of the Intergovernmental Panel on Climate Change*, Cambridge University Press, Cambridge.

Moore, D.F. (1975) *The Friction of Pneumatic Tyres*, 1st ed., Elsevier Scientific Publishing Company, New York.

Nordström, O. (1993) *The VTI Flat Bed Tyre Test Facility: A New Tool for Testing Commercial Tyre Characteristics*, SAE Paper 1993-933006, pp.1323, Reprinted from: The Influence of Tire, Axle and Brake Characteristics on Truck Braking and Steering Performance (SP 1003), Warrendale, USA.

Payne, A. (1962) 'The dynamic properties of carbon black-loaded natural rubber vulcanizates', *Journal of Applied Polymer Science*, Vol. 4, No. 19, pp.57–63.

SAE International (1976) *SAEJ670E. 'Vehicle Dynamics Terminology. Society of Automotive Engineers'*, Warrendale, USA.

Schuring, D. (1977) 'A new look at the definition of tire rolling loss', *Proceedings of Tire Rolling Losses and Fuel Economy – an R & D Planning Workshop*, Cambridge, USA, pp.31–38.

Svendenius (2007) *Tire Modeling and Friction Estimation*, PhD Dissertation, Lund University, Lund, Sweden.

Ydrefors, L., Hjort, M., Kharrazi, S., Jerrelind, J. and Stensson Trigell, A. (2021a) 'Rolling resistance and its relation to operating conditions: a literature review', *Proceedings of the Institution of Mechanical Engineers, Part D: Journal of Automobile Engineering*, Vol. 235, No. 12, pp.2931–2948, doi:10.1177/09544070211011089.

Ydrefors, L., Hjort, M., Kharrazi, S., Jerrelind, J. and Stensson Trigell, A. (2021b) 'Development of a method for measuring rolling resistance at different tyre temperatures', *Proceedings From the 27th IAVSD Symposium on Dynamics of Vehicles on Roads and Tracks*, 17–19 August, St. Petersburg, Russia.

Zener, C. (1948) 'Elasticity and anelasticity of metals', *J. Phys. Chem.*, p.53, https://doi.org/10.1021/j150474a017